Atmos. Chem. Phys. Discuss., 9, 1727–1756, 2009
www.atmos-chem-phys-discuss.net/9/1727/2009/

Atmospheric Chemistry and Physics Discussions

This discussion paper is/has been under review for the journal *Atmospheric Chemistry and Physics (ACP)*. Please refer to the corresponding final paper in *ACP* if available.

A two-step scheme for high-resolution regional atmospheric trace gas inversions based on independent models

C. Rödenbeck, C. Gerbig, K. Trusilova, and M. Heimann

Max Planck Institute for Biogeochemistry, P.O. Box 100164, 07701 Jena, Germany

Received: 1 September 2008 – Accepted: 21 November 2008 – Published: 19 January 2009

Correspondence to: C. Rödenbeck (christian.roedenbeck@bgc-jena.mpg.de)

Published by Copernicus Publications on behalf of the European Geosciences Union.

Abstract

Mixing ratio measurements of atmospheric tracers like CO_2 can be used to estimate regional surface-air tracer fluxes using inverse methods, involving a numerical transport model. Currently available transport models are either global but rather coarse, or more accurate but only over a limited spatial and temporal domain. To obtain higher-resolution flux estimates within a region of interest, existing studies use zoomed or coupled models. The two-step scheme developed here uses global and regional models sequentially in separate inversion steps, coupled only via the data vector. This provides a nested atmospheric inversion scheme without the necessity of a direct coupled model implementation. For example, the scheme allows an easy nesting of Lagrangian models with their potential of very high resolution into global inversions.

1 Introduction

"Atmospheric transport inversions" are a tool to estimate the surface-atmosphere exchange of biogeochemical trace gases based on atmospheric mixing ratio measurements and a numerical transport model. This method is widely used, e.g., for atmospheric CO_2 (Enting et al., 1995; Bousquet et al., 2000; Rödenbeck et al., 2003; Baker et al., 2006, and many others). Since atmospheric transport links any location on Earth within much less than one year, the inversion problem is intrinsically global, such that a global transport model and a global flux representation need to be used. On the other hand, both atmospheric transport and the source/sink patterns of CO_2 (or other biogeochemical species) have significant variability on fine spatial and temporal scales (less than kilometres or hours, especially over continents) – neglecting this variability leads to considerable errors in the flux retrievals (Gerbig et al., 2003a,b; van der Molen and Dolman, 2007; Pérez-Landa et al., 2007; Ahmadov et al., 2007). However, given present-day computing capabilities, atmospheric transport models are either global with grid resolutions of no finer than about $2^\circ \times 2^\circ$, or of finer scale (down to

about 2 km×2 km) but only for a limited spatial domain and temporal period. In the near future, we do not expect the availability of models that could combine high resolution and global/multi-year coverage.

Existing studies solve the problem by focusing on a domain of interest (DoI) and possibly a period of interest (PoI) over which fluxes and transport are finer resolved. This can be done using "zoomed" atmospheric transport models gradually refining the grid resolution towards the DoI (e.g., Peylin et al., 2005), or nested models with higher-resolution insets coupled along the boundary (e.g., Peters et al., 2007).

The two-step algorithm presented here has been designed with the following aims:

- The scheme is meant to allow completely independent models to be used for global and regional transport. "Independent" means that the two models do not need to be of similar type, and, even more importantly, the two models do not need to be run in a coupled mode (the implementation of nesting capabilities can be rather involved, and would be required for both the models and their adjoints). An envisaged application is the combination of a global Eulerian (gridded) model with a Lagrangian (backward trajectory) regional model to resolve the flux field in the vicinity of the observations with much higher spatial and temporal resolution at relatively low computational cost (Lin et al., 2003; Gerbig et al., 2003a).

- Nesting poses several issues, that need to be solved to sufficient approximation. Within the DoI, for a prescribed surface flux field, different models (or nests of the same model with different resolutions) will simulate different mixing ratio fields (e.g., Geels et al., 2007) – how to handle this mismatch? For a short PoI, how to spin up the atmospheric mixing ratio field from an unknown state? For example, Peylin et al. (2005) were able to solve the spin-up problem in a 1-month inversion using a SVD decomposition of the initial mixing ratio field. Additional degrees of freedom could also be introduced at the boundary (compare Lauvaux et al., 2008). The aim of the present scheme is to solve these issues as accurate as possible, but also with as few as possible changes to existing global or regional

single-model inversion schemes.

This paper describes the two-step recipe, and demonstrates it with the TM3 transport model run on different spatial resolutions. The example region (DoI) is Europe where a relatively dense observation network is available.

2 Method

2.1 Motivation

The global mixing ratio field $c^{glob}(\boldsymbol{x}, t)$ of a conservative atmospheric tracer, given its sources and sinks ("fluxes") $f(\boldsymbol{x}, t)$ and the atmospheric transport, is a solution of the three-dimensional, time-dependent continuity equation

$$\mathcal{T}[c^{glob}(\boldsymbol{x}, t)] = f(\boldsymbol{x}, t) \tag{1}$$

with initial conditions

$$c^{glob}(\boldsymbol{x}, t)|_{t=0} = c_{ini}(\boldsymbol{x}) \tag{2}$$

The transport operator $\mathcal{T}$ is given by

$$\mathcal{T}[\_] = \frac{\partial}{\partial t}\rho(\boldsymbol{x}, t)[\_] + \nabla \cdot \rho(\boldsymbol{x}, t)\boldsymbol{v}(\boldsymbol{x}, t)[\_] \tag{3}$$

where ρ denotes the air density and $\boldsymbol{v}$ the 3-D wind vector.

If the consideration is restricted to the domain of interest (DoI), the regional mixing ratio field $c^{reg}(\boldsymbol{x}, t)$ within the DoI is a solution of the same continuity Eq. (1), with the additional boundary condition

$$c^{reg}(\boldsymbol{x}, t) = c^{glob}(\boldsymbol{x}, t)|_{\boldsymbol{x}=\partial \mathrm{DoI}} \tag{4}$$

where ∂DoI stands for the border of the DoI. Since the transport operator $\mathcal{T}$ is linear in the mixing ratio, the solution within the DoI can be represented mathematically as the

sum of two unique components: (1) a homogeneous solution c^{reg}_{hom} with no fluxes in the DoI but which matches the boundary conditions on ∂DoI, and (2) a non-homogeneous solution c^{reg}_{nh} which has zero boundary conditions, but which is subject to the fluxes in the DoI, i.e.,

$$c^{reg} = c^{reg}_{hom} + c^{reg}_{nh} \tag{5}$$

where c^{reg}_{hom} and c^{reg}_{nh} are the solutions to

$$\begin{aligned} \mathcal{T}\left[c^{reg}_{hom}\right] &= 0, \qquad c^{reg}_{hom}(\boldsymbol{x},t) = c^{glob}(\boldsymbol{x},t)|_{\boldsymbol{x}=\partial\text{DoI}} \\ \mathcal{T}\left[c^{reg}_{nh}\right] &= f(\boldsymbol{x},t), \quad c^{reg}_{nh}(\boldsymbol{x},t) = 0|_{\boldsymbol{x}=\partial\text{DoI}} \end{aligned} \tag{6}$$

Physically, the two component solutions within the DoI can be interpreted as arising from different transport pathways of the tracer:

1. The non-homogeneous solution $c^{reg}_{nh}(\boldsymbol{x},t)$ is the mixing ratio of all the tracer substance that originated from source/sink locations within the DoI and the PoI and arrived at location $\boldsymbol{x}$ (within the DoI) and time t without ever leaving the DoI (hereafter called I→I pathways);

2. The homogeneous solution $c^{reg}_{hom}(\boldsymbol{x},t)$ is generated by any pathways from fluxes outside the domain and transported into the domain across the boundary (O→I pathways), or by any pathways that started inside the DoI, temporally left the DoI, and re-entered the DoI later across the boundary (I→O→I pathways).

An inversion estimates the fluxes f from a set of mixing ratio data, as sketched in Sect. 2.2 below. Eq. (6) shows that the fluxes inside the DoI, which are the target quantity of the regional inversion, are only related to the non-homogeneous contribution to the mixing ratio. The idea of the two-step scheme proposed here, therefore, is to first (approximately) remove the influence of the homogeneous contribution from the regional data. Then, in a second step, the regional inversion can simply be done with zero boundary conditions in the regional transport model.

2.2 General inversion scheme

Before describing the two-step approach in detail, we review the "ordinary" inversion process, thereby introducing the involved quantities. The method ("linear Bayesian inverse estimation") is used in many atmospheric trace gas studies. Some details of the present description refer to the implementation for CO_2 by Rödenbeck et al. (2003) and its extensions described in Rödenbeck (2005), but the nesting scheme should also be applicable to other implementations.

The primary input to the flux estimation is the observed mixing ratios $\boldsymbol{c}_{meas}$ (vector of all individual measured values at different times and locations). Modelled mixing ratios $\boldsymbol{c}_{mod}$ that arise from a given temporally and spatially varying discretized flux field $\boldsymbol{f}$ are computed by an atmospheric transport model. Formally, they can be written as[1]

$$\boldsymbol{c}_{mod} = \mathbf{A}\boldsymbol{f} + \boldsymbol{c}_{ini} \tag{7}$$

in terms of a transport matrix $\mathbf{A}$. The values in $\boldsymbol{c}_{mod}$ are sampled in the model for every individual time and location where there is a measured value in $\boldsymbol{c}_{meas}$.

The inversion calculation seeks those fluxes $\boldsymbol{f}$ that lead to the best match between observed and modelled mixing ratios, in the sense that the value of the cost function

$$J_c = \frac{1}{2}(\boldsymbol{c}_{meas} - \boldsymbol{c}_{mod})^{\mathsf{T}}\mathbf{Q}_c^{-1}(\boldsymbol{c}_{meas} - \boldsymbol{c}_{mod}) \tag{8}$$

is minimal. The (diagonal) matrix $\mathbf{Q}_c$ introduces a weighting among the mixing ratio values (here involving assumed measurement uncertainty, location-dependent model uncertainty, and a data density weighting Rödenbeck, 2005).

[1] The initial condition $\boldsymbol{c}_{ini}$ corresponds to a well-mixed atmosphere with a given initial tracer mixing ratio; the flux-related increments in mixing ratio since the start of the simulation will be denoted by

$$\Delta\boldsymbol{c}_{mod} = \boldsymbol{c}_{mod} - \boldsymbol{c}_{ini}$$

Generally, minimization of the above cost function would be an ill-posed problem, which is usually remedied by adding Bayesian a-priori constraints. This is done here by writing the flux field $\boldsymbol{f}$ as

$$\boldsymbol{f} = \boldsymbol{f}_{fix} + \mathbf{F}\boldsymbol{p} \tag{9}$$

("linear statistical flux model"). The vector $\boldsymbol{p}$ represents the set of adjustable parameters, each of which acts as a multiplier to one of the columns of the matrix $\mathbf{F}$. These columns represent elementary spatio-temporal flux patterns (like elementary flux pulses) composing the total flux. Mathematical stability of the flux estimation is ensured by adding a second term to the cost function,

$$J = J_c + \frac{1}{2}\boldsymbol{p}^{\mathrm{T}}\boldsymbol{p} \tag{10}$$

As the parameters $\boldsymbol{p}$ a-priori have zero mean, unit variance, and are uncorrelated, this corresponds to introducing a Bayesian a-priori probability distribution for $\boldsymbol{f}$ with mean ("best-guess") $\boldsymbol{f}_{fix}$ and covariance matrix $\mathbf{Q}_{\boldsymbol{f},pri}=\mathbf{F}\mathbf{F}^{\mathrm{T}}$. The cost function J is then minimized with respect to the parameters $\boldsymbol{p}$ (here using a Conjugate Gradients algorithm with re-orthogonalization, Rödenbeck, 2005).

2.3 Domains, periods, and transport models

The description of the nesting scheme needs the following terms as defined here:

Fluxes, transport, inversion runs, etc. will be considered either within the spatial domain of interest (DoI) or for the entire Earth surface (global).

In time, we will consider a period of interest (PoI), or a full period (FP) including at least some more time for spin-up. The PoI might be as short as one year or less. The spin-up time is chosen to be one year, corresponding to the mixing time of the global atmosphere.

The 2-step nesting scheme involves several independent transport models (symbolized here by their transport matrices):

$\mathbf{A}^{glob}_{coarse}$. A global transport model on a coarser resolution, that can be run for the full multi-year period (FP).

$\mathbf{A}^{reg}_{fine}$. A higher-resolution model simulating only the DoI (and only running during the PoI). The model is run with simple zero boundary (and initial) conditions, such that all tracer substance leaving the DoI is lost, and no tracer is (re-)entering over the boundary (i.e., it only simulates the non-homogeneous mixing ratio field arising from I→I pathways).

$\mathbf{A}^{reg}_{coarse}$. A manipulated version of the global model $\mathbf{A}^{glob}_{coarse}$, which mimics the regional model in only simulating the non-homogeneous mixing ratio field arising from I→I pathways (implemented here by setting the 3-D mixing ratio field outside the DoI/PoI to zero after every transport or emission time step).

$\mathbf{A}^{glob}_{fine}$. A hypothetical transport model that has both higher resolution and global coverage, as the conceptual benchmark.

2.4 The recipe of the two-step nesting scheme

To facilitate the following description, see Fig. 1 for an overview.

2.4.1 Step 1

The first step consists in an ordinary global inversion as of Sect. 2.2, done with all available data and the global transport model $\mathbf{A}^{glob}_{coarse}$. It yields global coarse-resolution flux estimates $\boldsymbol{f}_1$ over the FP.

2.4.2 Intermediate step: The "remaining mixing ratio"

Based on the results $\boldsymbol{f}_1$ of the step-1 inversion, two forward runs are performed:

1. A normal run of the global transport model (over the FP), yielding modelled mixing ratio increments

$$\Delta \boldsymbol{c}_{mod_1} = \mathbf{A}^{glob}_{coarse} \boldsymbol{f}_1 \tag{11}$$

(By construction, $\boldsymbol{c}_{mod_1} = \Delta\boldsymbol{c}_{mod_1} + \boldsymbol{c}_{ini}$ will closely match the data $\boldsymbol{c}_{meas}$.)

2. A run of the manipulated coarse-grid model $\mathbf{A}^{reg}_{coarse}$, starting with zero mixing ratio at the start of the PoI. The resulting modelled mixing ratio increments

$$\Delta\boldsymbol{c}_{mod_1,nh} = \mathbf{A}^{reg}_{coarse}\boldsymbol{f}_1 \tag{12}$$

will only give the non-homogeneous (I→I) contributions inside the DoI/PoI (and can be considered zero at all sites outside).

Then, a "remaining mixing ratio"

$$\Delta\boldsymbol{c}_{remain} = \boldsymbol{c}_{meas} - \underbrace{(\Delta\boldsymbol{c}_{mod_1} - \Delta\boldsymbol{c}_{mod_1,nh}}_{\Delta\boldsymbol{c}_{mod_1,hom}} + \boldsymbol{c}_{ini}) \tag{13}$$

is calculated for all observational sites inside the DoI/PoI. It represents the data diminished by the homogeneous mixing ratio as calculated by the global model from the fluxes $\boldsymbol{f}_1$.

2.4.3 Step 2

Finally, a second inversion run is performed, that differs from the step-1 inversion in two main aspects:

- The global model is replaced by the high-resolution regional transport model $\mathbf{A}^{reg}_{fine}$, and all fluxes are represented on fine resolution.
- The data $\boldsymbol{c}_{meas}$ are replaced by the "remaining mixing ratio" $\Delta\boldsymbol{c}_{remain}$.

In addition, some secondary changes are required, because the restriction of the fluxes to the DoI and PoI affects the a-priori correlation structure of the inversions. Details are described in Appendix A. In all other aspects, step 2 is just an ordinary inversion as step 1.

The results $\boldsymbol{f}_2$ of the step-2 inversion give the final high-resolution flux estimates within the DoI/PoI.

2.4.4 Benchmark

The conceptual benchmark for any nesting scheme are the results of an (ordinary) inversion with the global high-resolution transport model $\mathbf{A}_{fine}^{glob}$. Of course, this will not be feasible computationally in a real application. The global high-resolution flux estimates from the benchmark will be denoted $\boldsymbol{f}_B$, and the mixing ratios modelled from these fluxes using the same global high-resolution model are $\Delta\boldsymbol{c}_{mod_B}=\mathbf{A}_{fine}^{glob}\boldsymbol{f}_B$ (with $\Delta\boldsymbol{c}_{mod_B,nh}=\mathbf{A}_{fine}^{reg}\boldsymbol{f}_B$ and $\Delta\boldsymbol{c}_{mod_B,hom}=\Delta\boldsymbol{c}_{mod_B}-\Delta\boldsymbol{c}_{mod_B,nh}$ being their non-homogeneous and homogeneous contributions, respectively).

2.5 Demonstration examples

Two demonstration examples (tests A and B) have been performed to check the feasibility and the errors of the scheme. As the transport model, TM3 (Heimann and Körner, 2003) has been used, which can be run on different spatial resolutions. Thereby, $\mathbf{A}_{coarse}^{glob}$ is provided by the TM3 model on a coarser resolution, while TM3 on a finer resolution does provide a benchmark model $\mathbf{A}_{fine}^{glob}$ here. A "regional model" $\mathbf{A}_{fine}^{reg}$ is obtained by applying the cut-out manipulation (as for $\mathbf{A}_{coarse}^{reg}$, Sect. 2.3) to the higher-resolution model $\mathbf{A}_{fine}^{glob}$. The particular TM3 resolutions used in the examples are given in Table 1, together with the different time periods of the runs.

The two tests mainly differ in the kind of data: Test B uses real data, measured by various institutions. There are both flask data (mainly weekly sampling) and in-situ data (hourly averages, selected for day time and variability less than 1 ppm/h). In contrast, test A uses synthetic data created by a forward run of the global higher-resolution benchmark model $\mathbf{A}_{fine}^{glob}$. The fluxes used to create the pseudo-data ("known truth") comprise daily fossil fuel emissions, terrestrial net ecosystem exchange (NEE),

and ocean exchange[2]. Importantly, the time points and locations of the synthetic data are the same as those of the real data, such that they represent the same amount of atmospheric information as in a real inversion.

The domain of interest (DoI) in both tests is Europe and some surrounding areas (15° W–55° E, 30° N–85° N). The measurement sites are shown in Fig. 2 (Europe only; there are 68 sites globally)[3]. As target quantity of the inversions, we take the temporal variations of the fluxes integrated over 5 parts of the DoI (colored regions in Fig. 2).

The inversion set-up (used for both tests) is very similar to that described in Rödenbeck (2005). Land fluxes are estimated on pixel resolution, with exponentially decaying a-priori correlations on a scale of around 1000 km (ocean: 2×2 aggregated pixels and around 1300 km correlation scale). Temporally, the fluxes have daily resolution, with a-priori correlations on a weekly scale. Fixed (a-priori) fluxes comprise annual fossil fuel emissions (Olivier and Berdowski, 2001), a constant NEE field (long-term mean of the LPJ model, Sitch et al., 2000), and a constant ocean exchange field (from Gloor et al., 2003). The main difference to Rödenbeck (2005) is a slightly tighter a-priori constraint (sigmas smaller by factor 2.83). Moreover, there are no extra seasonal components, as they would make less sense for a 1-year inversion as in test B.

[2] Daily terrestrial NEE is taken from the BiomeBGC model (Trusilova and Churkina, 2008); daily fossil fuel emissions are from Olivier and Berdowski (2001) (with weekly and seasonal distribution functions), temporally extrapolated according to BP statistics (BP); and oceanic CO_2 fluxes come from an inversion of ocean interior carbon data (sum of the anthropogenic fluxes from Mikaloff Fletcher et al., 2006, the preindustrial fluxes from Mikaloff Fletcher et al., 2007, and the river fluxes of Jacobson et al., 2007). The exact choice of the "known truth" is however not critical.

[3] Note that the data records of some sites do not span the entire time period of test A. In a real inversion, this may lead to artificial variations in time (Rödenbeck et al., 2003), but it should not be a problem here as it would affect benchmark and two-step results in approximately the same way.

3 Results

3.1 Test A

Figure 3 shows flux time series from within the chosen DoI/PoI to be compared for test A. The results of a global inversion using the global higher-resolution model $\mathbf{A}^{glob}_{fine}$ (orange line) are taken as the benchmark fluxes to be approximated as good as possible. A global inversion with the coarser model $\mathbf{A}^{glob}_{coarse}$ (thin blue line) differs considerably from this benchmark, a difference entirely due to the transport model errors. However, when going from this step-1 inversion to the step-2 results $\boldsymbol{f}_2$ of the nesting scheme (thick purple line), the error is considerably reduced. Although the agreement in the temporal features with the benchmark is not perfect, the differences are now also rather small compared to the temporal flux variability itself.

Since synthetic data have been inverted here, the correct answer should be a reproduction of the fluxes ("known truth", black line) that have been used in the forward run creating the pseudo-data. Even the benchmark inversion, for which forward run and inversion use the same transport model such that transport is effectively perfect, is not fully able to reproduce the "known truth", reflecting inherent limitations of the inversion: the available information in the atmospheric data set is incomplete, and the adjustable degrees of freedom built into the estimation do not contain all features of the "known truth" (such as the small-scale and short-term variability). Important in the present context, however, is that the difference between the step-2 results and the benchmark are similar or smaller than their deviation from the "known truth": Thus, the nesting does not add a significant error to these inherent limitations.

3.2 Test B

This example tests the scheme in a situation closer to the real application: inverting measured data, using a higher resolution for the TM3 model in step 2, and running the high-resolution step only over 1 year. The results are shown without temporal filtering

in Fig. 4. Again, this test shows the clear improvements of the nested results over the results of the coarser-grid inversion.

4 Discussion

4.1 Suitability

The aim of any nesting scheme is to provide an approximation to a hypothetical high-resolution global inversion, where CPU demands are sufficiently reduced to make the calculation feasible, while the additional errors remain sufficiently small.

The computational gain arises here

- because the spin-up period is mainly taken care of by the coarse-resolution step 1, such that the PoI can be shorter;
- because less iterations are needed for convergence of the iterative solution (in test A, less than 20 rather than 30 to 40), due to the smaller number of constraints to be simultaneously satisfied;
- and, most importantly, because the regional model only has to be run within the DoI.

The size of the additional errors has been tested in the two examples. Even though these results necessarily only test specific flux features, they do suggest that the presented two-step nesting scheme approximates the high-resolution global inversion within the DoI with for practical purposes fully sufficient accuracy.

4.2 Rationale

With regard to the regional flux gradients/changes within the DoI, the "remaining mixing ratio" $\boldsymbol{c}_{remain}$ (Eq. 13) used in the step-2 inversion essentially contains the full

information from the data (cmp. Sect. 2.1). It is only diminished by the homogeneous contributions that cannot be handled by the zero-boundary regional model[4]. The situation is illustrated in Fig. 5 (especially by the mid-continental site Schauinsland in the right panels): The full modelled mixing ratios $\boldsymbol{c}_{mod_1}$ (green) fit all variability of the data $\boldsymbol{c}_{meas}$ (red) well due to the optimization in step 1. The homogeneous contribution $\boldsymbol{c}_{mod_1,hom}$ to the mixing ratio (blue) only represents smoother contributions advected from the boundary (including all the long-term trend), while the local (non-homogeneous) signals characterized by high synoptic variability stay in the "remaining mixing ratio" $\Delta\boldsymbol{c}_{remain}$. Closer to the inflow boundary (as at Mace Head shown in the left panels), $\Delta\boldsymbol{c}_{remain}$ is much smaller, corresponding to the fact that only a small part of the area of influence of Mace Head is covered by adjustable fluxes from inside the DoI.

Thus, inverting $\Delta\boldsymbol{c}_{remain}$ in step 2 successfully retrieves most of the within-DoI flux features. Deviations of the two-step approximation $\boldsymbol{f}_2$ from the global high-resolution benchmark $\boldsymbol{f}_B$ arise due to the errors in $\boldsymbol{c}_{mod_1,hom}$ (as calculated by the coarse transport model) with respect to the hypothetical values $\boldsymbol{c}_{mod_B,hom}$ when using the benchmark model (Sect. 2.4.4). However, even though the fluxes $\boldsymbol{f}_1$ inverted by the coarse model in step 1 will have considerable errors, the errors of $\boldsymbol{c}_{mod_1,hom}$ are expected to be small: The full modelled mixing ratio $\boldsymbol{c}_{mod_1}$ has a good match to the data by construction[5], and its split into homogeneous and non-homogeneous contributions should not

[4] These contributions include, obviously, any responses to fluxes from outside the DoI or from before the PoI (O→I pathways). Somewhat more subtle, however, they also include responses to fluxes from inside the DoI/PoI that however temporarily left the DoI (I→O→I pathways) – subtracting these as well is essential in order to remove the full long-term mixing ratio trend corresponding to the global flux (the regional model with zero boundary condition cannot accumulate any tracer over the years, thus it cannot handle the trend).

[5] This consideration also confirms that the "remaining mixing ratio" has to be calculated by the coarse model: Using, for example, a nested transport model (seemingly more accurate within the DoI) would cause a mismatch between inverse and forward runs, thereby increasing

ACPD
9, 1727–1756, 2009

be too model-dependent either (in particular as the more error-prone near-field contributions are cancelling out in $\Delta \boldsymbol{c}_{remain}$, at least away from the boundary). Figure 6 shows that this is indeed the case in the example A.

Deviations also arise from the edge effects to the a-priori correlation structure caused by the existence of the boundary. Of course, this will affect the flux estimates closer to ∂DoI more than those well inside, in dependence on the correlation lengths. When the tests were done using an inversion set-up with longer spatial correlations, the performance of the scheme indeed deteriorated. Choosing shorter a-priori correlations is thus advisable. Also, the domain of interest should be chosen carefully. In our examples, it is certainly advantageous that the western (inflow) boundary of the DoI lies in the ocean, such that no correlations of the land fluxes are cut off there; in general, the boundary should as far as possible cut in the ocean(land) for a land(ocean) focussed DoI. Also, nesting makes naturally most sense in an area with relatively high density of observation sites, able to sample the mixing ratio gradients within the DoI.

Corresponding to the agreement of the step-2 fluxes with the benchmark, also the residuals (deviation of the a-posteriori modelled mixing ratios from the data) at sites within the DoI are similar (e.g., Schauinsland in Fig. 7). Closer to the boundary, the improvement over step 1 is much smaller, as expected (e.g., Mace Head).

As step 2 is using again the mixing ratio data already used in step 1, the concern arises whether the assumptions required for applying Bayesian inference are violated. Formally, such a violation exists because the modelled mixing ratios ($\boldsymbol{c}_{mod_1,hom}$) and the data in Eq. (13) are not statistically independent, so their difference has a (co)variance different from that of the data alone. However, the fluxes within the DoI predominantly depend on spatial and temporal mixing ratio gradients within the domain, as contained in the data, while $\boldsymbol{c}_{mod_1,hom}$ mainly depends on the fluxes outside. Though there are correlations between the fluxes $\boldsymbol{f}_1$ inside and outside of the DoI, the successful flux retrieval in the tests suggests that the effect of these correlations is sufficiently small.

rather than decreasing the errors. (In addition, of course, the practical advantage of the two-step scheme not to require a coupled model would be lost.)

This is even more clearly confirmed by examining the calculated uncertainties of the a-posteriori fluxes (Fig. 8) because those would be affected by a wrong data (co)variance more strongly than the a-posteriori fluxes themselves. Nonetheless, Fig. 8 reveals only very small deviations of the uncertainties as calculated in the step-2 inversion relative to the benchmark: The deviations are not larger than the small changes in a-priori (co)variances due to the spatial cut-out. (Larger deviations do occur for areas closer to the eastern boundary of the DoI, but this is where the approximation fails anyway.) We conclude that the two-step scheme does not violate Bayesian assumptions to any practically relevant degree.

A forward model run based on the flux results of an ordinary inversion does not only yield mixing ratio values $\boldsymbol{c}_{mod_1}$ corresponding to the data, but a full 3-D mixing ratio field $c^{glob}_{mod_1}(\boldsymbol{x}, t)$ (that, in analogy to weather forecasting, could be called "analyzed" or "assimilated" mixing ratios). In the case of the two-step scheme, the corresponding 3-D mixing ratio field within the DoI is the sum of the homogeneous contribution calculated from step 1 and the (non-homogeneous) contribution from step 2,

$$c^{reg}_{mod_2}(\boldsymbol{x}, t) = c^{reg}_{mod_1,hom}(\boldsymbol{x}, t) + c^{reg}_{mod_2,nh}(\boldsymbol{x}, t) \quad (14)$$

where $c^{reg}_{mod_1,hom}(\boldsymbol{x}, t)$ can be obtained as a difference between full and non-homogeneous global fields.

5 Conclusions

This paper introduces a two-step scheme for high-resolution flux estimation, by spatio-temporal nesting of a domain of interest (DoI) and a period of interest (PoI) into a global and longer inversion. It does not require any zooming or nesting capabilities in modelling atmospheric transport. Only relatively minor work is needed to implement the scheme into an existing (single-model) inversion system:

– The global transport model needs the option to only simulate the non-homogeneous contribution within the DoI, e.g., by setting the mixing ratio field outside the DoI to zero after each model time step;

– suitable logic in the inversion system to replace the data by a difference of modelled mixing ratios ($\Delta \boldsymbol{c}_{remain}$);

– options to suitably manipulate the a-priori settings of the inversion to accommodate the cut-out spatial and temporal domain (see Appendix A).

Once done, essentially any pair of transport models can technically be nested. Potentially, also a further refinement by adding more steps on even higher resolution may be appropriate.

According to our test examples, the scheme provides within the domain of interest a very good approximation to the results of a hypothetical global high-resolution inversion. The functioning of the scheme can be understood mathematically in terms of homogeneous vs. non-homogeneous contributions to the solution of the tracer continuity equation within the regional domain.

Appendix A

In the implementation of the step-2 inversion, some secondary changes with respect to the usual inversion procedure are necessary:

– As the fluxes are only defined within the DoI, suitable modifications to the a-priori information are required along the boundary.

  In the flux model formulation used here (Rödenbeck, 2005), the spatial elements are cut at the boundary, such that the spatial correlations from inside to outside the DoI are disrupted; the pointwise normalization of the elements restores the a-priori sigma intervals of the individual pixels. As our implementation also involves a normalization according to the a-priori sigmas of specific linear flux functionals

(that extend beyond the DoI and short PoI's), corrective scaling factors had to be applied to ensure that the pixel-wise a-priori sigmas are equal to that in the global flux model.

- The inversion runs only over the PoI (implying minor changes to the temporal correlation structure near the start/end of the PoI).
- The initial mixing ratio (at the start of the PoI) is zero, and any degrees of freedom related to adjustments of the initial mixing ratio are removed.

Note: In the step-2 inversion, both data and fluxes are only defined within the DoI/PoI. In the numerical implementation, however, it does not harm to keep the data outside the DoI because this would just add a constant offset to the cost function J_c irrelevant to the minimization. Likewise, if convenient, the flux fields may be implemented globally because any fluxes outside the DoI would not interfere with the step-2 estimation.

Acknowledgements. We would like to thank S. Mikaloff-Fletcher for kindly providing the oceanic fluxes used to create the pseudo-data. Stimulating discussions with P. Peylin and S. Houweling are gratefully acknowledged.

This Open Access Publication is financed by the Max Planck Society.

References

Ahmadov, R., Gerbig, C., Kretschmer, R., and et al: Mesoscale covariance of transport and CO2 fluxes: Evidence from observations and simulations using the WRF-VPRM coupled atmosphere-biosphere model, J. Geophys. Res.-Atmos., 112, D22107, doi:10.1029/2007JD008552, 2007. 1728

Baker, D. F., Law, R. M., Gurney, K. R., Rayner, P., Peylin, P., Denning, A. S., Bousquet, P., Bruhwiler, L., Chen, Y.-H., Ciais, P., Fung, I. Y., Heimann, M., John, J., Maki, T., Maksyutov, S., Masarie, K., Prather, M., Pak, B., Taguchi, S., and Zhu, Z.: TransCom 3 inversion intercomparison: Impact of transport model errors on the interannual variability of regional CO2 fluxes, 1988–2003, Global Biogeochemical Cycles, 20, GB1002, doi:10.1029/2004GB002439, 2006. 1728

Bousquet, P., Peylin, P., Ciais, P., Le Quéré, C., Friedlingstein, P., and Tans, P. P.: Regional changes in carbon dioxide fluxes of land and oceans since 1980, Science, 290, 1342–1346, 2000. 1728

BP: Statistical Review of World Energy June 2006, available at http://www.bp.com/statisticalreview, 2006. 1737

Enting, I., Trudinger, C. M., and Francey, R. J.: A synthesis inversion of the concentration and $\delta^{13}C$ of atmospheric CO_2, Tellus, 47B, 35–52, 1995. 1728

Geels, C., Gloor, M., Ciais, P., Bousquet, P., Peylin, P., Vermeulen, A. T., Dargaville, R., Aalto, T., Brandt, J., Christensen, J. H., Frohn, L. M., Haszpra, L., Karstens, U., Rödenbeck, C., Ramonet, M., Carboni, G., and Santaguida, R.: Comparing atmospheric transport models for future regional inversions over Europe - Part 1: mapping the atmospheric CO_2 signals, Atmos. Chem. Phys., 7, 3461–3479, 2007, http://www.atmos-chem-phys.net/7/3461/2007/. 1729

Gerbig, C., Lin, J., Wofsy, S., Daube, B. C., Andrews, A. E., Stephens, B. B., Bakwin, P. S., and Grainger, C. A.: Toward constraining regional-scale fluxes of CO2 with atmospheric observations over a continent: 1. Observed spatial variability from airborne platforms, J. Geophys. Res.-Atmos., 108, 4756, doi:10.1029/2002JD003018, 2003a. 1728, 1729

Gerbig, C., Lin, J., Wofsy, S., Daube, B. C., Andrews, A. E., Stephens, B. B., Bakwin, P. S., and Grainger, C. A.: Toward constraining regional-scale fluxes of CO2 with atmospheric observations over a continent: 2. Analysis of COBRA data using a receptor-oriented framework, J. Geophys. Res.-Atmos., 108, 4757, doi:10.1029/2003JD003770, 2003b. 1728

Gloor, M., Gruber, N., Sarmiento, J., Sabine, C. L., Feely, R. A., and Rödenbeck, C.: A first estimate of present and preindustrial air-sea CO_2 flux patterns based on ocean interior carbon measurements and models, Geophysical Research Letters, 30, 1010, doi:10.1029/2002GL015594, 2003. 1737

Heimann, M. and Körner, S.: The global atmospheric tracer model TM3, Tech. Rep. 5, MPI BGC, Jena (Germany), 2003. 1736

Jacobson, A. R., Fletcher, S. E. M., Gruber, N., Sarmiento, J. L., and Gloor, M.: A joint atmosphere-ocean inversion for surface fluxes of carbon dioxide, I: Methods and global-scale fluxes, Global Biogeochem. Cycles, 21, GB1019, doi: 10.1029/2005GB002556, 2007. 1737

Lauvaux, T., Uliasz, M., Sarrat, C., Chevallier, F., Bousquet, P., Lac, C., Davis, K. J., Ciais, P., Denning, A. S., and Rayner, P. J.: Mesoscale inversion: first results from the CERES campaign with synthetic data, Atmos. Chem. Phys., 8, 3459–3471, 2008, http://www.atmos-chem-phys.net/8/3459/2008/. 1729

Lin, J., Gerbig, C., Wofsy, S., and et al: A near-field tool for simulating the upstream influence of atmospheric observations: The Stochastic Time-Inverted Lagrangian Transport (STILT) model, J. Geophys. Res.-Atmos., 108, 4493, doi:10.1029/2002JD003161, 2003. 1729

Mikaloff Fletcher, S. E., Gruber, N., Jacobson, A. R., Doney, S. C., Dutkiewicz, S., Gerber, M., Follows, M., Joos, F., Lindsay, K., Menemenlis, D., Mouchet, A., Mller, S. A., and Sarmiento, J. L.: Inverse estimates of anthropogenic CO2 uptake, transport, and storage by the ocean, Global Biogeochem. Cycles, 20, GB2002, doi:10.1029/2005GB002530, 2006. 1737

Mikaloff Fletcher, S. E., Gruber, N., Jacobson, A. R., Doney, S. C., Dutkiewicz, S., Gerber, M., Gloor, M., Follows, M., Joos, F., Lindsay, K., Menemenlis, D., Mouchet, A., Müller, S. A., and Sarmiento, J. L.: Inverse estimates of the oceanic sources and sinks of natural CO2 and the implied oceanic transport, Global Biogeochem. Cy., 21, GB1010, doi:10.1029/2006GB002751, 2007. 1737

Olivier, J. G. J. and Berdowski, J. J. M.: Global emissions sources and sinks, In: The Climate System, edited by: Berdowski, J., Guicherit, R., and Heij, B. J., A. A. Balkema Publishers/Swets & Zeitlinger Publishers, Lisse, The Netherlands, ISBN-90-5809-255-0, 33–78, 2001. 1737

Pérez-Landa, G., Ciais, P., Gangoiti, G., Palau, J. L., Carrara, A., Gioli, B., Miglietta, F., Schumacher, M., Millán, M. M., and Sanz, M. J.: Mesoscale circulations over complex terrain in the Valencia coastal region, Spain – Part 2: Modeling CO_2 transport using idealized surface fluxes, Atmos. Chem. Phys., 7, 1851–1868, 2007, http://www.atmos-chem-phys.net/7/1851/2007/. 1728

Peters, W., Jacobson, A. R., Sweeney, C., Andrews, A. E., Conway, T. J., Masarie, K., Miller, J. B., Bruhwiler, L. M. P., Pétron, G., Hirsch, A. I., Worthy, D. E. J., van der Werf, G. R., Randerson, J. T., Wennberg, P. O., Krol, M. C., and Tans, P. P.: An atmospheric perspective on North American carbon dioxide exchange: CarbonTracker, PNAS, 104, 18 925–18 930,

2007. 1729

Peylin, P., Rayner, P. J., Bousquet, P., Carouge, C., Hourdin, F., Heinrich, P., Ciais, P., and AEROCARB contributors: Daily CO_2 flux estimates over Europe from continuous atmospheric measurements: 1, inverse methodology, ACP, 5, 3173–3186, 2005. 1729

Rödenbeck, C.: Estimating CO_2 sources and sinks from atmospheric mixing ratio measurements using a global inversion of atmospheric transport, Tech. Rep. 6, MPI BGC, Jena (Germany), http://www.bgc-jena.mpg.de/mpg/websiteBiogeochemie/Publikationen/Technical_Reports/tech_report6.pdf, 2005. 1732, 1733, 1737, 1743

R—"odenbeck, C., Houweling, S., Gloor, M., and Heimann, M.: CO_2 flux history 1982-2001 inferred from atmospheric data using a global inversion of atmospheric transport, Atmos. Chem. Phys., 3, 1919–1964, 2003, http://www.atmos-chem-phys.net/3/1919/2003/. 1728, 1732, 1737

Sitch, S., Prentice, I., Smith, B., Cramer, W., Kaplan, J., Lucht, W., Sykes, M., Thonicke, K., and Venevsky, S.: LPJ – a coupled model of vegetation dynamics and the terrestrial carbon cycle, in: The role of vegetation dynamics in the control of atmospheric CO_2 content (S. Sitch, PhD Thesis), Lund University, Lund (Sweden), 2000. 1737

Trusilova, K. and Churkina, G.: The terrestrial ecosystem model BIOME-BGC v1, Tech. Rep. 14, MPI BGC, Jena (Germany), http://www.bgc-jena.mpg.de/bgc-systems/publications/tech_report14.pdf, 2008. 1737

van der Molen, M. and Dolman, H.: Regional carbon fluxes and the effect of topography on the variability of atmospheric CO_2, J. Geophys. Res.-Atmos., 112, D01104, doi:10.1029/2006JD007649, 2007. 1728

Table 1. Characteristics of the two test inversions (for their detailed meaning see Sect. 2).

	Test A	Test B
TM3 res.[a] $\mathbf{A}^{glob}_{coarse}$, $\mathbf{A}^{reg}_{coarse}$	≈8°×10°	≈8°×10°
TM3 res.[a] $\mathbf{A}^{reg}_{fine}$, $\mathbf{A}^{glob}_{fine}$	≈4°×5°	≈1.8°×1.8°
Period of interest (PoI)[b]	2000–2006	2006
Full period (FP)[b]	1999–2006	2005–2006
Data	synthetic[c]	measurements

[a] Resolution given as latitude×longitude

[b] Years inclusive

[c] Synthetic mixing ratios are used at the same time instants and locations as the measurements.

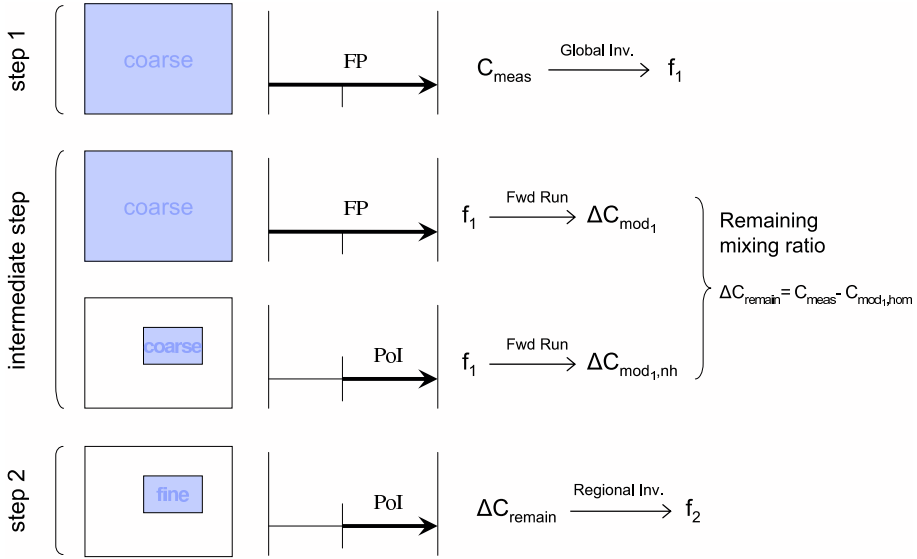

Fig. 1. Schematic overview of the individual steps of the algorithm described in Sect. 2.4.

ACPD
9, 1727–1756, 2009

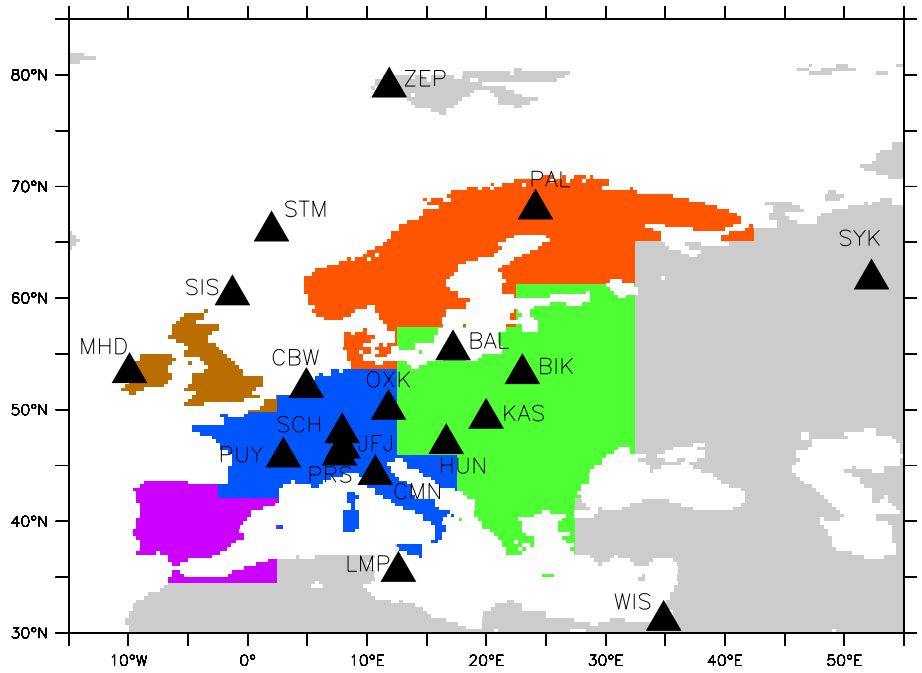

Fig. 2. Map of the domain of interest (DoI) of the example inversions, showing the measurement sites used in the estimation, as well as the integration regions for post-processing.

ACPD
9, 1727–1756, 2009

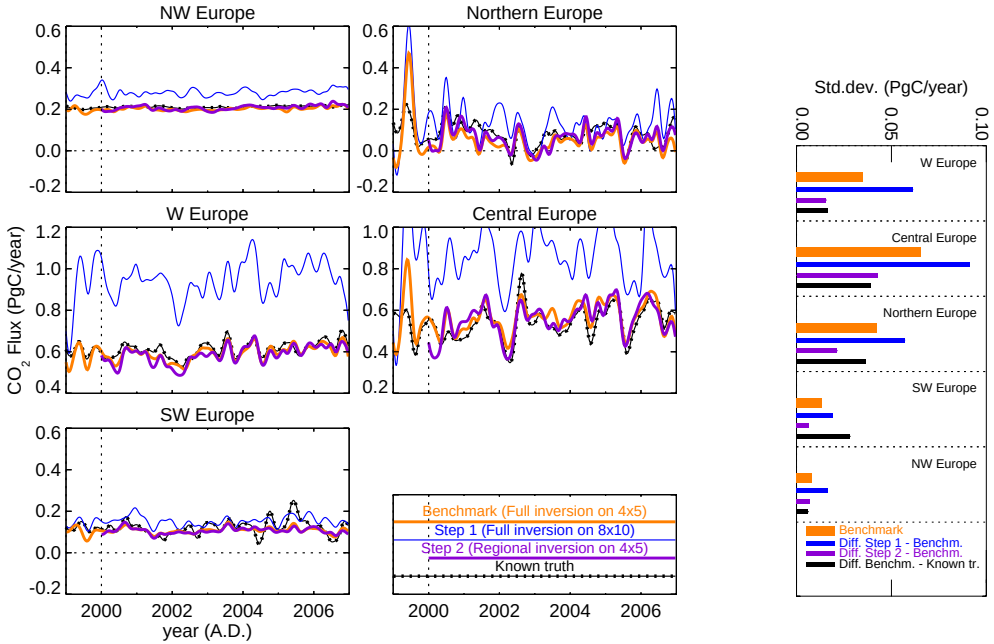

Fig. 3. Results of test A: *Time series:* Comparing the results of the benchmark inversion, steps 1 and 2 of the nested inversion, and the "known truth" used to create the synthetic data. Fluxes have been integrated over 5 parts of Europe (colored regions in Fig. 2), deseasonalized (by subtracting the mean seasonal cycle over 2001–2005 [incl.]), and 3-monthly filtered (Gaussian spectral weights).
Bars: Temporal standard deviations of the differences between the step-1 results, the step-2 results, or the "known truth", and the benchmark results (narrow bars). The standard deviation of the benchmark fluxes themselves is given as a reference of the signal size (wide bar). (Temporal standard deviations have been calculated from the filtered fluxes over the PoI; they do not incorporate the differences in mean.)

ACPD
9, 1727–1756, 2009

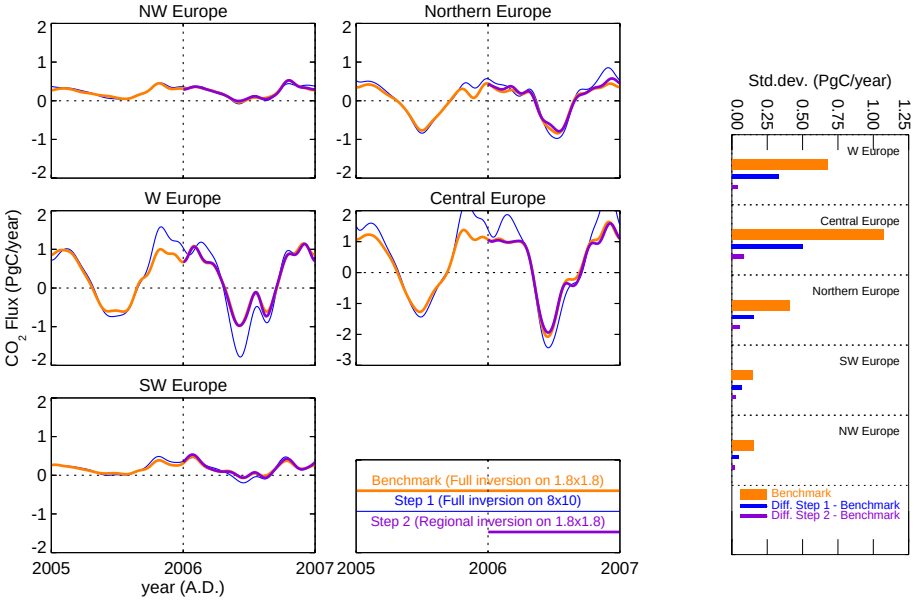

Fig. 4. Results of test B. Fluxes have been integrated over 5 parts of Europe as in Fig. 3, but not filtered temporally.

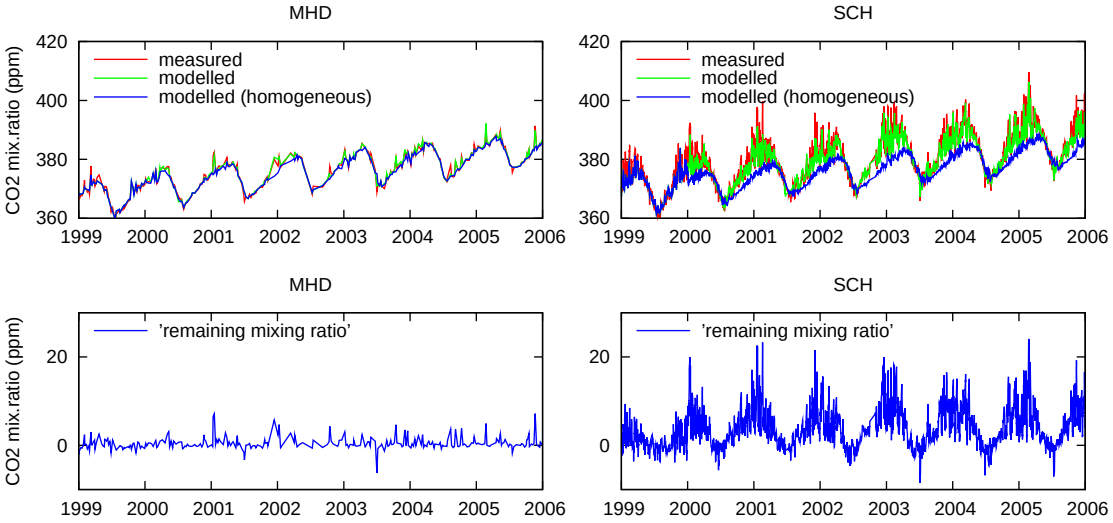

Fig. 5. Examples to illustrate the construction of the "remaining mixing ratio", at Mace Head close to the western inflow boundary (MHD, flask data) and at Schauinsland in the center of the DoI (SCH, hourly data). Top panels: Time series of measured mixing ratio ($\boldsymbol{c}_{meas}$, red), modelled mixing ratio after step 1 ($\boldsymbol{c}_{mod_1}$, green), and its homogeneous contribution $\boldsymbol{c}_{mod_1,hom}$ (i.e., modelled without I→I pathways, blue). Bottom panels: The "remaining mixing ratio" ($\boldsymbol{c}_{meas}-\boldsymbol{c}_{mod_1,hom}$).

ACPD
9, 1727–1756, 2009

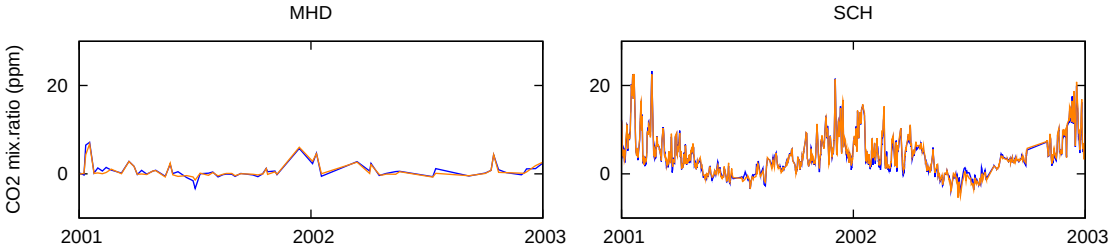

Fig. 6. Comparison of the "remaining mixing ratio" as calculated in step 1 ($\boldsymbol{c}_{meas}-\boldsymbol{c}_{mod_1,hom}$, blue as in Fig. 5) with the corresponding quantity from the benchmark inversion ($\boldsymbol{c}_{meas}-\boldsymbol{c}_{mod_B,hom}$, orange).

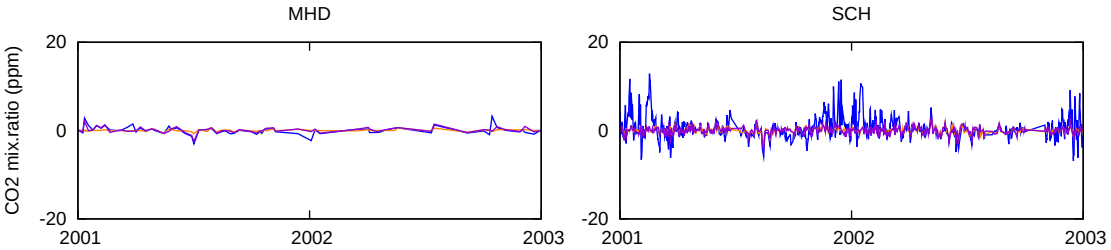

Fig. 7. Comparison of the residuals of the step-2 inversion ($\boldsymbol{c}_{meas}-\boldsymbol{c}_{mod_2}$, violet) with those of the benchmark inversion ($\boldsymbol{c}_{meas}-\boldsymbol{c}_{mod_B}$, orange) and of the step-1 inversion ($\boldsymbol{c}_{meas}-\boldsymbol{c}_{mod_1}$, blue).

ACPD
9, 1727–1756, 2009

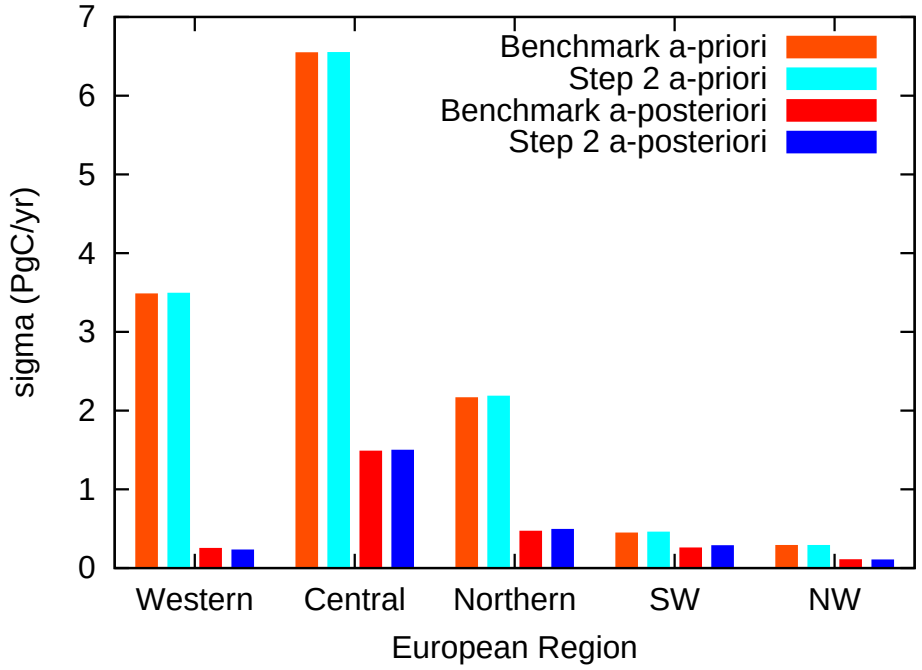

Fig. 8. A-priori and a-posteriori uncertainty intervals for regionally integrated and temporally filtered fluxes (as in Fig. 3), as calculated by the benchmark inversion and the regional approximation.